An optoelectronic framework enabled by low-dimensional phase change films

Peiman Hosseini[1], C. David Wright[2] and Harish Bhaskaran[1]*

[1] Department of Materials, University of Oxford, Parks Road, Oxford OX1 3PH (United Kingdom).
[2] College of Engineering, Mathematics and Physical Sciences, University of Exeter, Harrison Building, North Park Road, Exeter EX4 4QF (United Kingdom).

* E-mail: harish.bhaskaran@materials.ox.ac.uk

Abstract

The development of materials whose refractive index can be optically transformed at will, such as chalcogenide-based phase change materials, have revolutionized the media and data storage industries by providing inexpensive, high-speed, portable and reliable platforms able to store vast quantities of data. Phase change materials switch between two solid states, amorphous and crystalline, in response to a stimulus, such as heat, with an associated change in the physical properties of the material including optical absorption, electrical conductance and Young's modulus[1-5]. The initial applications of these materials (particularly the alloy $Ge_2Sb_2Te_5$) exploited the reversible change in their optical properties in rewritable optical data storage technologies[6, 7]. More recently, the change in their electrical conductivity has also been extensively studied in the development of non-volatile phase change memories[4, 5]. In this article, we demonstrate for the very first time that by combining the optical *and* electronic property modulation of such materials, exciting display and data visualization applications beyond data storage can be created. Using extremely thin phase change materials and transparent conductors, we demonstrate electrically induced stable colour changes in both reflective and semi-transparent modes. Further, we showcase how a pixelated approach can be employed in displays on both rigid

and flexible films. Our results establish a novel optoelectronic framework using low-dimensional phase change materials with many likely applications such as ultra-fast (>MHz), entirely solid state, nanometre-scale pixelated micro and nano displays, semi-transparent smart glasses, smart contact lenses and artificial retina devices.

Phase Change Materials (PCM) have thus far played a key role in enabling the creation of a versatile platform able to store vast amounts of information on inexpensive plastic substrates (DVDs and other optical media[6, 7]) using optical pulses. These technologies employ light of specific wavelengths (for example, Blu-Ray at 405 nm, DVDs at 650 nm and CDs at 780 nm) to write and read data. The next generation of electronic, solid state memories based on phase change materials are set to potentially replace the current leading storage technologies, namely Flash and magnetic discs. Phase change materials[1-5] have become a leading candidate due to their extraordinary properties such as extreme scalability, fast switching speeds, and high switching endurance[4, 5]. However, although phase change materials have been commercialized in both the electrical[4] and optical domain[8], there has been very little work in understanding how transforming the phase in one domain affects the properties in another (i.e. how switching electrically affects optical properties, and vice-versa). This is because the likely applications emerging from such non-volatile, optoelectronic properties have thus far been unclear. In this article, we propose and demonstrate these optoelectronic properties in the context of very compelling and entirely novel display and data visualization applications.

Recently, thin-film perfect absorbers in the mid-IR have been demonstrated, where the optical properties of a temperature transient phase change material (VO_2) were tuned [9]. VO_2 however is stable in each of its phases only within certain temperature ranges, a

property that makes it energy inefficient and impractical to implement in electrically controlled circuits at the nanoscale. In contrast, the primary phases of $Ge_2Sb_2Te_5$ (GST), viz. amorphous and crystalline, are stable for most applications[10] and can be thermally, optically or electrically switched at ultra-high speed[11, 12]. Furthermore, GST is extremely scalable[13, 14], easily integrated in commercial devices and with optical properties that can be tuned in the visible spectrum of light[15]. In this article we describe a unique optoelectronic framework technology employing GST-based thin films and experimentally demonstrate its wide-ranging applicability in various types of display technologies. We show how such a system, when combined with a transparent electrode such as Indium Tin Oxide (ITO), can be used as a reflective or a semi-transparent micro-display and on both rigid and flexible substrates, which could usher in an era of truly flexible electronic screens that can operate at the maximum possible resolution allowed by the diffraction of visible light, both as back-lit displays as well as electronic readers. Current micro-display technologies based on liquid crystals, Microelectromechanical Systems (MEMS) and Organic Light Emitting Diodes (OLED) are attracting considerable attention because of a growing interest in wearable technology[16]. Key requirements for such applications are high resolution, high-speed and low power consumption, all of which are readily addressed by the technology that we describe in this article.

We first describe the reflective-type display using GST-based thin-films. Figure 1a shows the cross sectional schematic of our reflective type devices; the GST is sandwiched between two ITO layers and deposited on top of a reflective surface such as platinum. The crystallization of the few nanometre thick GST layer induces a colour change in the entire film, visible when incident “white” light is reflected back. To understand the relationship

between the thickness of the ITO and GST layers and the overall optical properties of the stack we systematically compute the reflectivity spectra of the stack while gradually increasing the thickness of each layer. Every calculation is undertaken two times, one for each phase of the GST layer; a change in the refractive index of the GST layer (caused by a change in phase) modulates the reflective spectrum of the entire stack. The spectra are finally compared and the change in reflectivity is plotted as $\Delta R_{\%} = \left(\frac{\boldsymbol{R_{crystal} - R_{amorphous}}}{\boldsymbol{R_{amorphous}}} \cdot 100\right)$, with $R_{crystal}$ being the reflectivity (at a specific wavelength) of the entire stack when the GST layer is in the crystalline phase and $R_{amorphous}$ the reflectivity when the GST layer is in the amorphous phase. We use the above expression because the amorphous phase provides the background. These models (top graphs in Figures 1b) indicate that one key factor is the presence of a transparent conductor beneath the GST (t in Figure 1d) which we refer to as the ITO spacer. This layer is crucial and contributes to the colour in our system as explained later in this article.

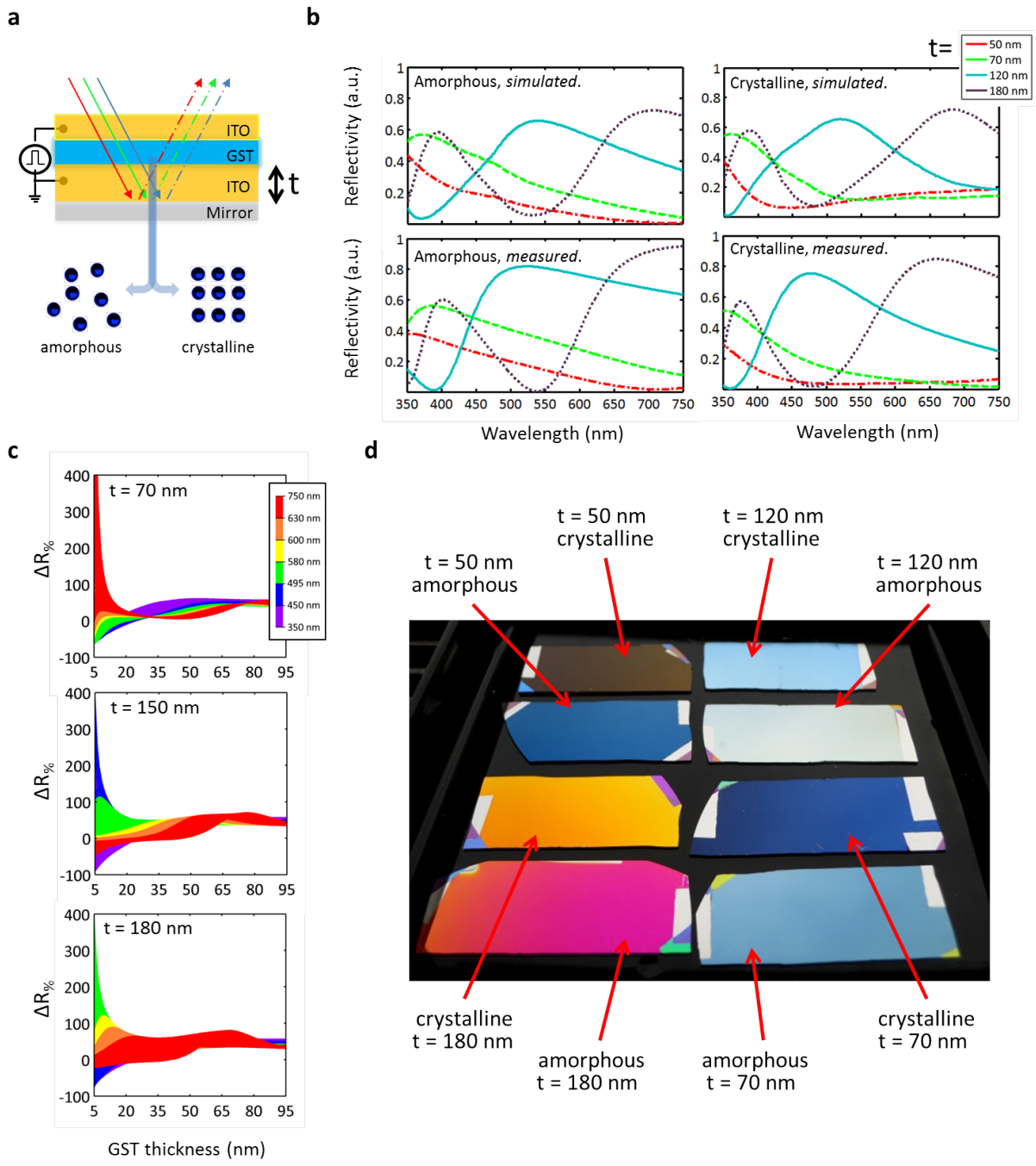

Figure 1

In order to experimentally verify our reflectivity calculations, we sputter a number of multi-layered films on Si wafers with 300 nm SiO_2; our GST layer is known to be amorphous as sputtered (S4, supplementary information). Figure 1d shows a photograph of a few

sputtered films with similar structure (10 nm ITO / 7 nm amorphous GST / ***t*** nm ITO / 100 nm Pt / SiO_2); *t* is the only thickness that is varied. The dramatic variation in the colour of the films when *t* (the ITO spacer thickness) is varied further demonstrates the importance of this layer. To fully crystallize the GST, we heat each sample up to 220˚ C for a few minutes on a hot plate. The observed variation in the colour of these samples when the GST is crystallized is also shown in Figure 1d; the colour variations are dramatic, showing the potential for such films for use as individual pixels in display devices, each pixel being a different colour to achieve a standard colour display device (and with switching in real devices achieved electrically, as we later demonstrate).

To quantify this colour change, we first model the system using a transfer matrix optical computational method[17] to calculate properties such as reflectance, transmittance and internal electrical field at visible wavelengths (full details of the model are available in S5, supplementary information). We then carry out reflectivity measurements on sputtered films to compare our model with experiments; we use a spectrometer (Lambda 1050, Perkin Elmer US) to obtain the reflectivity spectra of the samples both prior to and after crystallization. Figure 1b shows exceptionally good agreement between the simulated (top, left) and measured (bottom, left) reflectivity spectra for the samples shown in Figure 1d, when the thin GST layer is in the amorphous phase. Similar reflectivity spectra are shown (Figure 1b, right) for the same samples after crystallizing the GST layer, where again the agreement between experiment and theory is very good. These results show that an effective change in the reflectivity spectrum (i.e. colour) of the stack can be induced by simply changing the phase of a few nanometre thick chalcogenide layer.

The next aspect of our study focuses on the influence of the GST thickness. In conventional optical discs, the thickness of the GST layer is optimised, along with the thicknesses of surrounding dielectric layers, to enhance the optical contrast; however, the GST thicknesses used in commercial discs are relatively high (several tens of nanometres, typically). In the case of the films shown in Figure 1d, the thickness of the GST layer is just 7 nm (the very minimum we could sputter reliably using our facilities). Counter intuitively, as we explain below, smaller thicknesses enhance contrast dramatically and, importantly, lead to lower power electrical switching. Figure 1c shows our computational study of the change (shown as percentage) in optical reflectivity for various thicknesses of the ITO spacer and with increasing thickness of the phase change layer. For a thin layer of GST (i.e. below 20 nm) the range of wavelengths that show increased reflectivity upon crystallization varies depending on the chosen thickness of the ITO spacer. This allows the perceived colour of the entire stack to be transformed by simply changing the phase of a few nanometre thick GST layer. Interestingly this crystallization induced variation of reflectivity is exponentially amplified for thinner layers of the phase change material. Also, by tailoring the thickness of the ITO spacer, the reflectivity of specific wavelengths is enhanced when white light is used as illumination source. Figure 1c shows three examples with ITO thicknesses of 70, 150 and 180 nm where the red, green and blue components respectively are enhanced with the remaining wavelengths either decreased or weakly increased. The importance of the ITO spacer is further elucidated in S7, supplementary information where the absence of interference (i.e. no ITO spacer is inserted between the GST and the Pt layer) causes the reflectivity of the film to only weakly increase in the crystalline phase, mostly independent of

the wavelength. Experimental results confirming how these thicknesses influence reflectivity are presented later in this article.

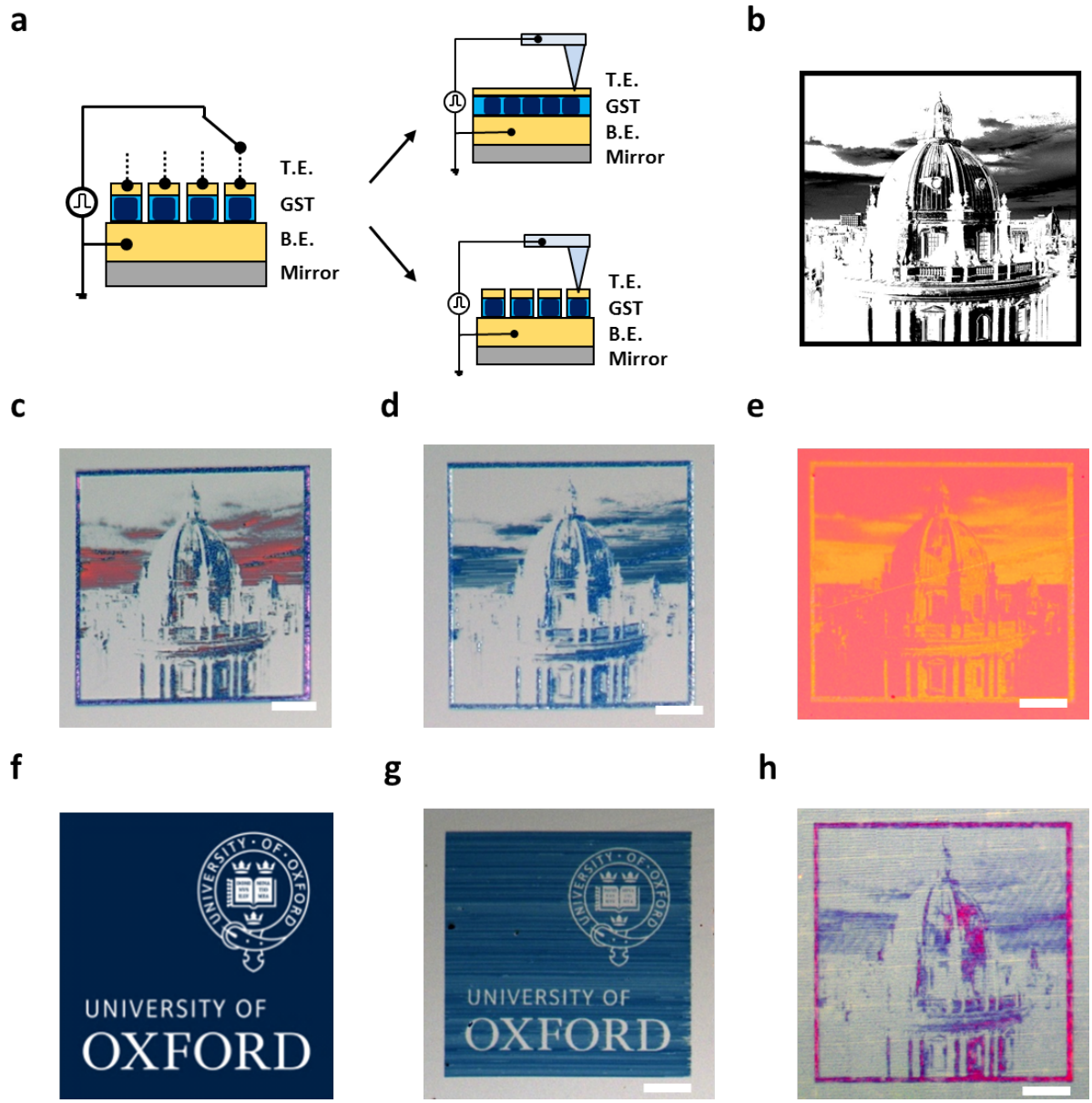

Figure 2

We now demonstrate how this thin-film stack could be used in future phase change materials-based display applications. To demonstrate the working principle of a display that can be electrically switched, we pattern an image using a nanometre sized electrical probe

(i.e. the conductive tip of an atomic force microscope, CAFM), which was previously shown capable of switching nanoscale crystalline areas[18-20] in phase change material films. Our technique uses a pixelated approach mimicking real pixels in actual devices (the fabrication of one of which we describe later in the article). The use of CAFM to characterize the nanoscale switching characteristics of phase change materials from the more amorphous to more crystalline phase has been studied previously, and is known to closely resemble a standard cross-bar phase change memory cell; hence we employ this technique to demonstrate our electrically enabled display technology[18, 21]. More details regarding this technique and how it relates to actual PCM-based devices (pixels) can be found in S1, supplementary information. To demonstrate the high optical contrast, we start by electrically drawing Oxford's Radcliffe Camera (a building, the grayscale image of which is shown in in Figure 2b) in Figure 2 c, d and e on similar films with 50 nm, 70 nm and 180 nm ITO spacer thickness respectively. All the pictures are clearly visible using a standard, non-polarized, optical microscope. It is important to note that no artificial contrast or colour has been added in postproduction. The striking contrast is readily visible demonstrating the feasibility of such ultra-thin phase change material based micro-displays. To demonstrate the colour-rendering capability, a different pattern representing the University of Oxford logo (shown in Figure 2f) is also electrically drawn on a 20 nm ITO / 7 nm GST / 70 nm ITO / 100 nm Pt. The resulting optical image is shown in Figure 2g, which closely matches the original logo, representing the Oxford "blue" in Figure 2f (the authors are aware that logos of author institutions are vastly overused; however we only do this to showcase our technology's colour performance, and draw your attention to the huge contrast between the blue and white regions).

We then verify that a pixelated array, as would be necessary in a display where each pixel can be randomly accessed and manipulated, is approximated very closely by our CAFM approach. To perform this verification, we fabricate an array of 300 nm × 300 nm pixels with 200 nm pitch on a standard vertical stack with a 50 nm thick ITO spacer. The active volume of each phase change cell (i.e. the GST layer) is restricted to a single pixel precisely addressable by the nanoscale tip. These were electrically switched using a nanoscale conductive tip. Figure 2h shows the resulting optical image, where the optical contrast is once again striking, confirming the validity of this demonstration. Further experiments using electrically switched single pixels, together with the resulting high optical contrast, are shown in supplementary information S1.

We now move on to transparent type substrates and electrically modulate their optical transmission. Future semi-transparent displays will find applications in exciting emerging technologies such as contact lens-type displays[22], smart eye glasses, windshield displays, for modulating light transmission through windows[23] or even for synthetic retina devices[24]. Such light modulation, achievable with resolution beyond the diffraction limit, is also important for future ultra-fast phase modulators, where a white light behind the semi-transparent display is selectively diffracted to produce interference. We now demonstrate how an ITO / GST / ITO structure could also be used in this semi-transparent display mode. For such a configuration the reflective platinum under-layer is not deposited and the entire structure is sputtered directly on top of a transparent substrate, quartz in our case. As in the previous case of reflective displays, the electrically induced crystallization (and re-amorphization) can be utilized as a means to create optical contrast.

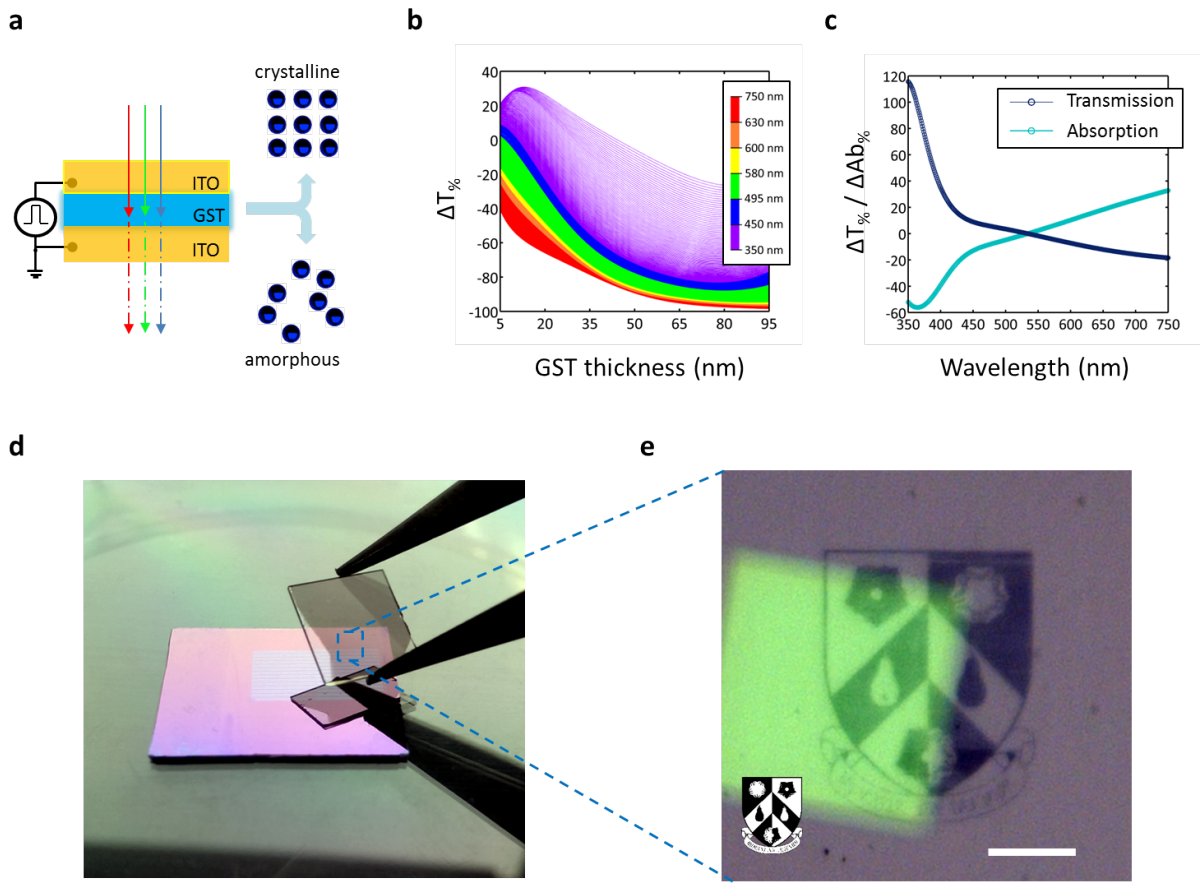

Figure 3

Figure 3a shows a schematic of the principle behind semi-transparent, phase change-based, displays. The calculated change in transmission (shown as percentage) between the amorphous and crystalline phase is shown in Figure 3b. According to the model a GST thickness of around 75 nm to 85 nm gives the highest change in transmission for most wavelengths however, due to the intrinsic absorption of the GST layer, the opacity of the films quickly drops after a few nanometres (further details are available in S6, supplementary information). We therefore choose a 7 nm GST layer sandwiched between 20 nm ITO and 40 nm ITO as best compromise between contrast and transparency. We also confirm the calculated change in absorption and transmission characteristics of such a film (shown in Figure 3c) by measuring and comparing its transmission (or absorption) spectra

upon crystallization. We then proceed to use the CAFM (similar to the experiments on reflective substrates of the previous section) to render pixelated images on these substrates. Figure 3e shows an example of an electrically constructed image, on such a substrate. To illustrate the transmissivity of the substrate, a square shaped green pad is placed underneath the rendered image; the transmissivity modulation is visible in Figure 3d and Figure 3e (the logo of Wolfson College, University of Oxford) and the contrast and transparency of the electrically drawn image is clearly seen. This demonstrates the principle of using such phase change optoelectronic frameworks for transmissive micro and nanodisplay applications, from electronic displays on windows, to backlit displays and as future wavelength tuneable windows.

The final demonstration of our technology is on flexible substrates. Given the extremely low thickness of our films, we find that they are amenable to flexible films (and therefore flexible displays). The development of a low power, ultra-thin flexible display has been a long-term worldwide goal, and the use of ITO could even enhance the possibility of using them as touch-sensitive displays. Figure 4a shows a picture of a 20 nm ITO / 7 nm GST / 50 nm ITO / 100 nm Pt multi-layered film on PET. The flexibility of these films with the sputtered layers is demonstrated in Figures 4a, c and d. The colour variation in these flexible reflective type displays is entirely similar to that on rigid substrates described earlier (Figure 2). Once again, we render images using a nanoscale conductive probe, and the resulting image is shown in Figure 4b. Although the quality of the PET substrate is much inferior to that of semiconductor grade SiO_2 or quartz, the electrically written high-resolution image of the Oxford Radcliffe Camera is readily visible. Another example of a similar film with a 180 nm ITO spacer is shown in Figure 4c, where the colour is now closer to yellow, which once

again shows the range of colours that are possible. As demonstrated earlier on rigid substrates, the use of such flexible films in semi-transparent modes is also possible. It is also remarkable that there is no visible colour variation when the films are bent, suggesting that such thin films also can be used as wide-viewing-angle displays. A semi-transparent, flexible film is shown in Figure 4d completing the demonstration for reflective and semi-transparent type displays on rigid, flexible and transparent substrates.

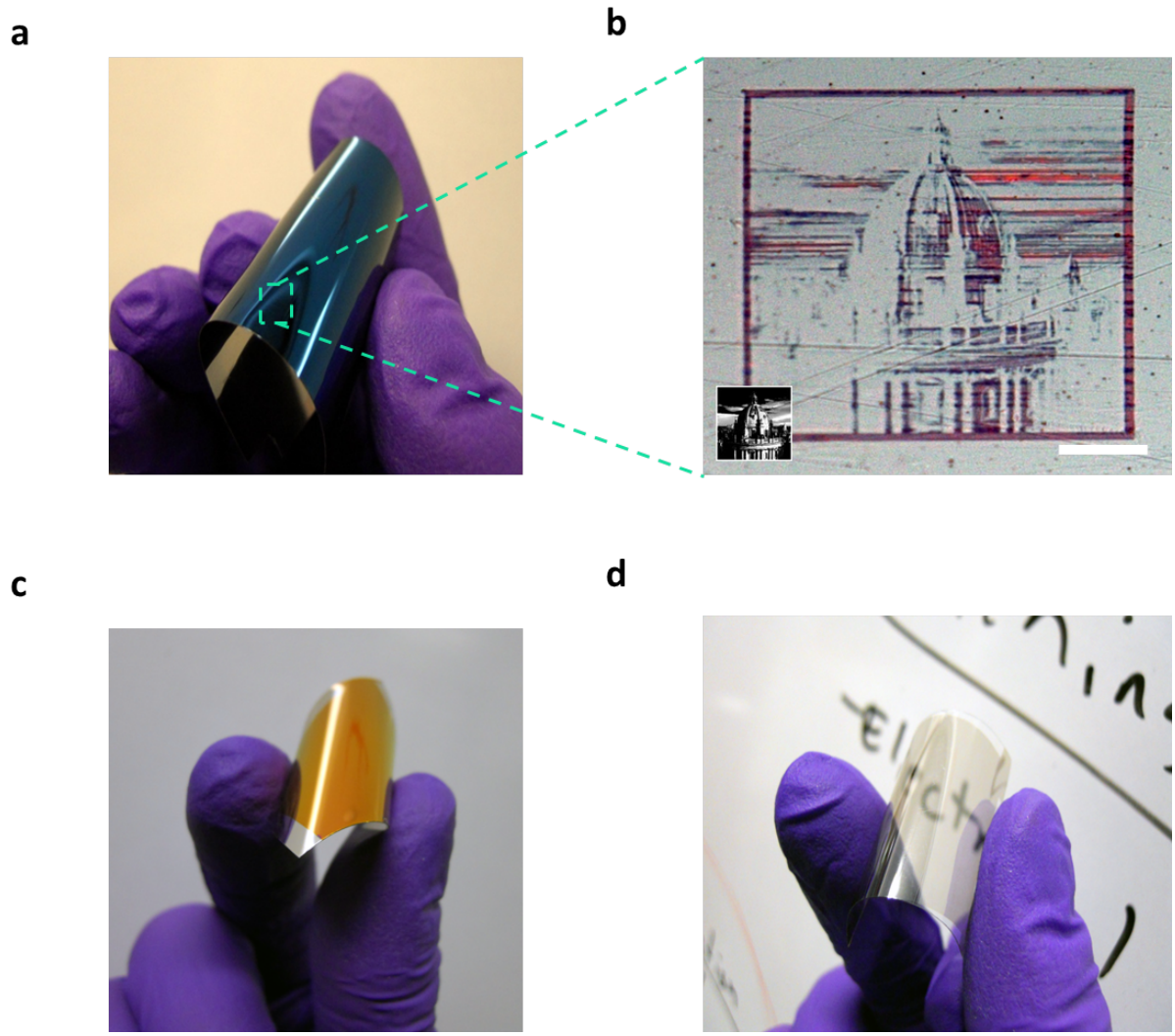

Figure 4

In all the above examples we use a CAFM to electrically switch the GST sandwiched between two ITO layers. Because no device using ITO electrodes has yet been demonstrated, we proceed to show that such a device (a single pixel) can be made and switched. Using a combination of electron beam lithography (EBL), reactive ion etching (RIE) and sputtering deposition, we fabricate vertical, crossbar like ITO/GST/ITO devices in order to test their electrical switching characteristics. We fabricate these devices on 300 nm SiO_2 on Si substrates (full details of the fabrication process are available in S3, supplementary information, with further consideration on the use of ITO as active electrode in S1). An optical image of a few crossbar devices is shown in Figure 5a with a falsely coloured magnified Scanning electron microscopy (SEM) image of one such device in the inset. This particular device has an active area (defined by the area of overlapping crossbars) of 300 nm × 300 nm. It is worth noting that switching in phase change memories is often restricted to nanometric regions of the cell[25]. The use of nanometre scale devices (pixels) is therefore preferable since full crystallization and re-amorphization of the pixel is required to enhance these novel optoelectronic functionalities. The electrical switching characteristics of such devices have been tested for various test cells with an example shown in Figure 5b-c. This particular cell shows a threshold voltage[26] of 2.2 V with a 350-times increase in conductance between the amorphous and crystalline phases. Figure 5b shows a collection of DC I/V curves used to transform the device to the high conductance (low resistance or crystalline phase) state (referred to in PCM devices as the SET state). 100 ns pulses with a fall-time of 5 ns and amplitude of 5V are used to transform the device to its initial low conductance (high resistance or amorphous) state (referred to as the RESET in PCM devices) state. A collection of SET/RESET iterations is shown in Figure 5c demonstrating its

repeatability (the cycle endurance of our devices will obviously require further engineering to create a commercial system, but we note that commercial-type phase change memories with endurances of greater than 10^8 have been demonstrated[27]). It is clear that our device is a single pixel (of very high resolution), and it is reasonable to expect that such a pixel can be replicated for display applications.

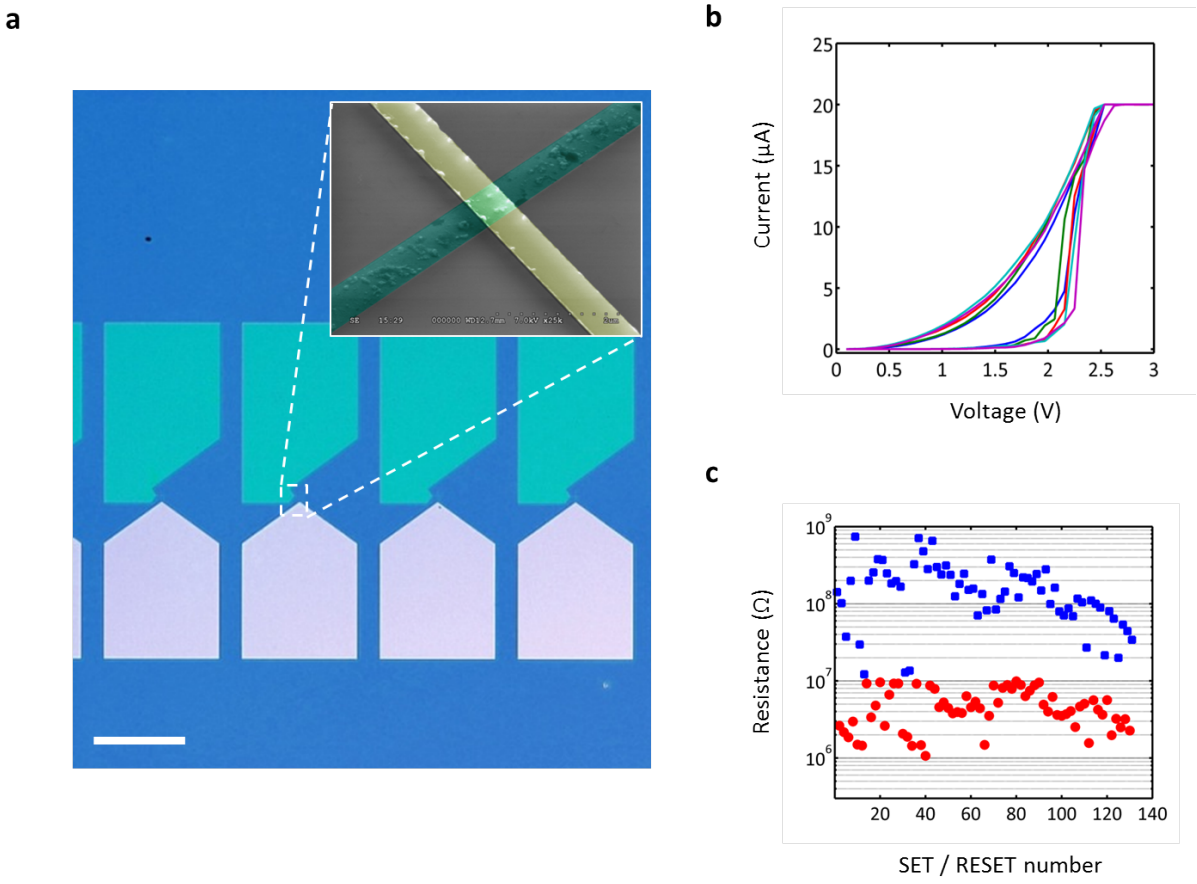

Figure 5

We now address the energy requirements for such a display using the results obtained from the single pixel device. In phase change memories the highest energy consumption is in the re-amorphization of a cell where sufficient energy is required to melt the phase change material[4]. We estimate the energy required to re-amorphize a single ITO

/ GST / ITO cell to be 15 pJ based on our experimental results. A 300 cm^2 display with 200 nm cell size and 50 nm gap between each cells would thus require 7.2 J to completely re-amorphize, similar to electrochromic devices[28]. The development of even thinner phase change materials would enable the energy consumption of a device (pixel) to be drastically reduced by 10 to a 100 times[13] which would also increase the optical contrast as already discussed. This would enable the use of phase change based electronic paper also as dynamic displays with few constraints on power requirements and ultra-high (>MHz) switching speed. Crucially for power consumption, no energy is required after a switching event, giving a net-zero-power consumption in static mode, a further improvement over existing colour back-lit micro-displays. Our results in this section thus demonstrate that such cells can be fabricated, are reliable and can be switched reversibly with low powers. Many challenges remain, especially in understanding how larger pixels can be switched most effectively and yet display optical contrast, as well as in arraying and sub-dividing pixels effectively to create any arbitrary colour and grey-scale. The use of growth-dominated phase change materials may prove to be a very useful approach in this respect, although their optoelectronic properties also remain unexplored and could be the subject of further research in this field.

In conclusion we have demonstrated a highly unique optoelectronic framework based on low dimensional phase change material films. The integration of a phase change material as an active switching layer in displays paves the way for a new class of smart devices that are both electrically and optically active. Our results represent the first applications of the electro-optical properties of such materials. The key result that we present is that very thin layers of phase change materials can display very high optical

contrast upon switching between the amorphous and crystalline phases when layered in appropriately designed thin film structures. Furthermore, because this can be done electrically, it allows for the fabrication of large arrays to create displays with ultra-high resolution. We demonstrate such displays on reflective and transparent substrates both on rigid and flexible surfaces; results that promise truly foldable ultralight displays that consume no power in static mode. We then further demonstrate the fabrication of one single pixel of a phase change cell with transparent electrodes. Because phase change materials are also capable of storing data and performing arithmetic and logic, such devices could potentially mimic the functionality of photoreceptor cells in the human eye opening up new fields of research in human-machine interaction, novel types of multi-functional glasses, contact lenses and synthetic retina devices. Further research into such ultra-thin materials and their optoelectronic properties would enable greater understanding of their potential for applications in these emerging technological areas.

Methods

Film deposition: Films are sputtered directly on thermally grown SiO_2 wafers (IDB Technology, UK), boPET (Mylar) or Quartz. Substrates were cleaned for 10 minutes in acetone under ultrasonic agitation, rinsed in isopropanol and dried with pressurized nitrogen. Where a reflector was needed (reflective type devices), 100 nm Pt was deposited using a Nordiko sputtering system: starting pressure 4.7×10^{-7} Torr, working pressure 1.6 mTorr, 30 sccm Ar, 400 W DC, 9 rpm. The samples were then moved to a second sputtering system for ITO and GST deposition. ITO is sputtered from a solid target (Testbourne, UK) using 25 W DC, 1.1 mTorr working pressure, 4×10^{-6} Torr starting pressure, 100˚C sample temperature at a

rate of 2 nm/min. Substrate heating is found to greatly reduce final surface roughness, increase optical transparency and electrical conductivity. $Ge_2Sb_2Te_5$ is sputtered from a solid target (Super Conductors Materials, USA) at 25 W DC, 1.1 mTorr working pressure, 4×10^{-6} Torr starting pressure and a rate of 8.5 nm/min, immediately following the ITO deposition in vacuum.

Optical characterization: Films were measured using a Lambda 1050 spectrometer (Perkin Elmer, US) in reflection, absorption and transmission using wavelengths between 350 nm and 750 nm. Reflectivity measurements were calibrated against a commercial Al standard.

Transfer matrix method: We employ a transfer matrix method described by Heavens[29] and successfully applied to various systems[17, 30]. More information can be found in supplementary information, S5.

Nanoscale patterning of continuous films and pixels: Patterns are generated by converting a selected grey scale image into a spatially resolved voltage pattern. An Asylum Research MFP-3D atomic force microscope (AFM) equipped with an ORCA accessory (modified to sustain our higher currents) and a conductive tip (DDESP, Bruker) is used as a nanoscale tip to electrically render several images on both films and pixels as shown in Figure 2a.

References

1. M. Wuttig, Phase-change materials - Towards a universal memory? *Nat Mater* **4**, 265-266 (Apr, 2005).
2. M. H. R. Lankhorst, B. W. S. M. M. Ketelaars, R. A. M. Wolters, Low-cost and nanoscale non-volatile memory concept for future silicon chips. *Nat Mater* **4**, 347-352 (Apr, 2005).
3. Y. C. Chen *et al.*, Ultra-thin phase-change bridge memory device using GeSb. *2006 IEDM*, 531-534 (2006).

4. S. Raoux *et al.*, Phase-change random access memory: A scalable technology. *Ibm J Res Dev* **52**, 465-479 (Jul-Sep, 2008).

5. M. A. Caldwell, R. G. D. Jeyasingh, H. S. P. Wong, D. J. Milliron, Nanoscale phase change memory materials. *Nanoscale* **4**, 4382-4392 (2012).

6. E. Ohno, N. Yamada, T. Kurumizawa, K. Kimura, M. Takao, Tegesnau Alloys for Phase-Change Type Optical Disk Memories. *Jpn J Appl Phys 1* **28**, 1235-1240 (Jul, 1989).

7. C. N. Afonso, J. Solis, F. Catalina, C. Kalpouzos, Ultrafast Reversible Phase-Change in Gesb Films for Erasable Optical Storage. *Appl Phys Lett* **60**, 3123-3125 (Jun 22, 1992).

8. M. Wuttig, N. Yamada, Phase-change materials for rewriteable data storage. *Nat Mater* **6**, 824-832 (Nov, 2007).

9. M. A. Kats, R. Blanchard, P. Genevet, F. Capasso, Nanometre optical coatings based on strong interference effects in highly absorbing media. *Nat Mater* **12**, 20-24 (Jan, 2013).

10. J. L. M. Oosthoek *et al.*, Evolution of cell resistance, threshold voltage and crystallization temperature during cycling of line-cell phase-change random access memory. *J Appl Phys* **110**, (Jul 15, 2011).

11. D. Loke *et al.*, Breaking the Speed Limits of Phase-Change Memory. *Science* **336**, 1566-1569 (Jun 22, 2012).

12. W. J. Wang *et al.*, Engineering Grains of Ge2Sb2Te5 for Realizing Fast-Speed, Low-Power, and Low-Drift Phase-Change Memories with Further Multilevel Capabilities. *2012 IEDM*, (2012).

13. F. Xiong, A. D. Liao, D. Estrada, E. Pop, Low-Power Switching of Phase-Change Materials with Carbon Nanotube Electrodes. *Science* **332**, 568-570 (Apr 29, 2011).

14. S. H. Lee, Y. Jung, R. Agarwal, Highly scalable non-volatile and ultra-lowpower phase-change nanowire memory. *Nat Nanotechnol* **2**, 626-630 (Oct, 2007).

15. N. Yamada, T. Matsunaga, Structure of laser-crystallized Ge2Sb2+xTe5 sputtered thin films for use in optical memory. *J Appl Phys* **88**, 7020-7028 (Dec 15, 2000).

16. N. Collings, T. Davey, J. Christmas, D. P. Chu, B. Crossland, The Applications and Technology of Phase-Only Liquid Crystal on Silicon Devices. *J Disp Technol* **7**, 112-119 (Mar, 2011).

17. G. F. Burkhard, E. T. Hoke, M. D. McGehee, Accounting for Interference, Scattering, and Electrode Absorption to Make Accurate Internal Quantum Efficiency Measurements in Organic and Other Thin Solar Cells. *Adv Mater* **22**, 3293–3297 (Aug 10, 2010).

18. O. Bichet, C. D. Wright, Y. Samson, S. Gidon, Local characterization and transformation of phase-change media by scanning thermal probes. *J Appl Phys* **95**, 2360-2364 (Mar 1, 2004).

19. H. Satoh, K. Sugawara, K. Tanaka, Nanoscale phase changes in crystalline Ge2Sb2Te5 films using scanning probe microscopes. *J Appl Phys* **99**, (Jan 15, 2006).

20. H. F. Hamann, M. O'Boyle, Y. C. Martin, M. Rooks, K. Wickramasinghe, Ultra-high-density phase-change storage and memory. *Nat Mater* **5**, 383-387 (May, 2006).

21. H. Bhaskaran, A. Sebastian, A. Pauza, H. Pozidis, M. Despont, Nanoscale phase transformation in Ge2Sb2Te5 using encapsulated scanning probes and retraction force microscopy. *Rev Sci Instrum* **80**, (Aug, 2009).

22. A. R. Lingley *et al.*, A single-pixel wireless contact lens display. *J Micromech Microeng* **21**, (Dec, 2011).

23. A. Llordes, G. Garcia, J. Gazquez, D. J. Milliron, Tunable near-infrared and visible-light transmittance in nanocrystal-in-glass composites. *Nature* **500**, 323-326 (Aug 15, 2013).

24. E. Zrenner, Fighting Blindness with Microelectronics. *Science Translational Medicine* **5**, 210ps216 (November 6, 2013, 2013).

25. S. W. Nam *et al.*, Electrical Wind Force-Driven and Dislocation-Templated Amorphization in Phase-Change Nanowires. *Science* **336**, 1561-1566 (Jun 22, 2012).

26. A. Redaelli, A. Pirovano, A. Benvenuti, A. L. Lacaita, Threshold switching and phase transition numerical models for phase change memory simulations. *J Appl Phys* **103**, (Jun 1, 2008).

27. R. Bez, P. Cappelletti, G. Servalli, A. Pirovano, Phase Change Memories Have Taken The Field. *2013 5th Ieee International Memory Workshop (Imw)*, 13-16 (2013).

28. J. Heikenfeld, P. Drzaic, J. S. Yeo, T. Koch, A critical review of the present and future prospects for electronic paper. *J Soc Inf Display* **19**, 129-156 (Feb, 2011).

29. O. Heavens, Optical Properties of Thin Solid Films. *J Opt Soc Am* **56**, 985 (1966).

30. L. A. A. Pettersson, L. S. Roman, O. Inganas, Modeling photocurrent action spectra of photovoltaic devices based on organic thin films. *J Appl Phys* **86**, 487-496 (Jul 1, 1999).

Figure 1 – Colour tuneability using few nanometres phase change materials: a, Schematic representation of our thin-film material stack comprising ITO / GST / ITO. The crystallization of the few nanometre thick GST layer induces a colour change in the entire film, visible when incident white light is reflected back. **b**, Simulated (top, left) and measured (bottom left) reflectivity spectra of the amorphous samples together with the simulated

(top, right) and measured (bottom, right) reflectivity spectra of the crystalline samples shown in d. In both phases, the close match between the model and simulation is striking. **c**, Change in reflectivity simulated for visible wavelengths, for various thicknesses of the ITO spacer and with increasing thickness of the GST layers. Each graph represents the change in optical reflectivity $(R_{crystal}-R_{amorphous})/R_{amorphous}\cdot 100)$ when the phase change material embedded in the ITO/GST/ITO/Pt structure is switched from amorphous to crystalline phase. By tailoring the thickness of the ITO spacer, the reflectivity of specific wavelengths is enhanced, and the remaining wavelengths are either decreased or weakly increased, when white light is used for illumination. **d**, An example of four different films with similar layered structure (starting from the topmost layer) consisting of 10 nm ITO / 7 nm GST / *t* nm ITO / 100 nm Pt) with different thicknesses of *t*, the ITO layer deposited between the GST and the reflective Pt layer. As can be seen, the value of *t* determines the reflected colour. After the deposition process, one part of each sample is placed on a hot plate at 220˚ C for a few minutes to induce complete crystallization of the GST layer. The corresponding colour change is also visible, and is quite dramatic. For example, the white (*t*=120nm) amorphous film turns light blue when crystallized. No post-production colour is added to enhance contrast.

Figure 2 – Reflective type display films: a, Schematic illustration of the electrically induced colour changes in phase change based electronic displays. **b**, The original (greyscale) picture of the Oxford Radcliffe Camera used as a pattern. **c**, Electrically constructed image on a continuous ITO/GST/ITO/Pt stack with 50 nm ITO spacer; the white regions are regions where the phase is amorphous. No artificial contrast has been added in postproduction. The pattern is once again electrically reproduced on various stacks with ITO spacer thickness of **d**, 70 nm and **e**, 180 nm. Scale bars are 10 μm, which show the ultimate resolution such displays are capable of achieving. **f**, The original image of the University of Oxford logo is used as a different pattern. **g**, Electrically constructed image on a ITO/GST/ITO/Pt stack with 70 nm ITO spacer – the blue regions are regions where the phase is transformed. **h**, To verify the effectiveness of our blanket film approach we electrically transformed an array of lithographically defined 300 nm x 300 nm pixels (200 nm pitch) on a standard vertical stack with a 50 nm thick ITO spacer; the optical contrast is strikingly evident, experimentally confirming that the pixelated array is well approximated by a CAFM generated one.

Figure 3 – Semi-transparent display type films: a, Schematic diagram of the principle behind a semi-transparent device using a ITO/GST/ITO structure on quartz. **b**, Computed change in optical transmission $\left(\frac{T_{crystal}-T_{amorphous}}{T_{amorphous}} \cdot \mathbf{100}\right)$, at different wavelengths, when the GST layer is switched between the amorphous and crystalline phases. **c**, Measured change, upon crystallization, in absorption and transmission spectra of a 20 nm ITO / 7 nm GST / 40 nm ITO film sputtered on quartz. **d**, A picture of the film measured in c. **e**, Microscope picture of an electrically constructed image on the film, demonstrating the principle of semi-transparent phase change material based electronic paper displays,. The green pad shown underneath the image comes from a sample placed underneath and it is used to demonstrate the semi-transparent nature and enhance clarity (because of the finite thickness of our transparent substrate, it is not in focus). Scale bar is 50 µm, once again highlighting the high resolution that is possible.

Figure 4 – Flexible type display films in both reflective and semi-transparent mode: a, Reflective type device on mylar showing flexibility as well as the wide angle colour stability of such films (i.e. when the film is bent, the colour in the bent region is not dramatically different). **b**, An electrically defined image is patterned directely on top of the flexible substrate using a CAFM as previously described, **c**, Further example of reflective type stack. **d**, A semi-transparent type structure sputterd directely on a flexible PET substrate.

Figure 5 – Demonstration of a single pixel: a, Optical image of a few ITO / GST / ITO crossbar like devices with a falsely coloured SEM micrograph of one single device in inset. Scale bar is 100 µm. **b**, A collection of various I/V curves demonstrating amorphous to crystalline switching behaviour of several ITO/GST/ITO cells. These particular devices displays a threshold voltage of ~2.2 V with a decrease in resistance of ~350 times when switched from the amorphous to the crystalline phase. The maximum current was limited to 20 µA. **c**, SET/RESET cycling of the same device. DC sweeps (similar to those in b above) are used to switch the device from the RESET (high resistance) state to the SET (low resistance) state. Several pulses of 5 V in amplitude with 100 ns width, 20 ns rising and 5 ns trailing edges, are used to switch the device back from the SET state to the RESET state.

Acknowledgements

The authors thank Robert Taylor for scientific discussions related to optical spectroscopy measurements. We are grateful to Moritz Riede for discussions on the modelling aspects of our study. This research was supported by EPSRC via grants EP/J018783/1, EP/J018694/1 and EP/J00541X/2 as well as the OUP John Fell Fund.

Contributions

All authors contributed substantially to this work. P.H. and H.B. conceived and designed the experiments. P.H. performed the experiments with inputs from H. B and C .D. W. All authors analysed the data. The manuscript was written by P.H. and H.B. with inputs from C.D.W.

Additional information

Supplementary information is available. Correspondence and requests for materials and devices should be addressed to H.B.

Competing financial interests

The authors declare no competing financial interests.

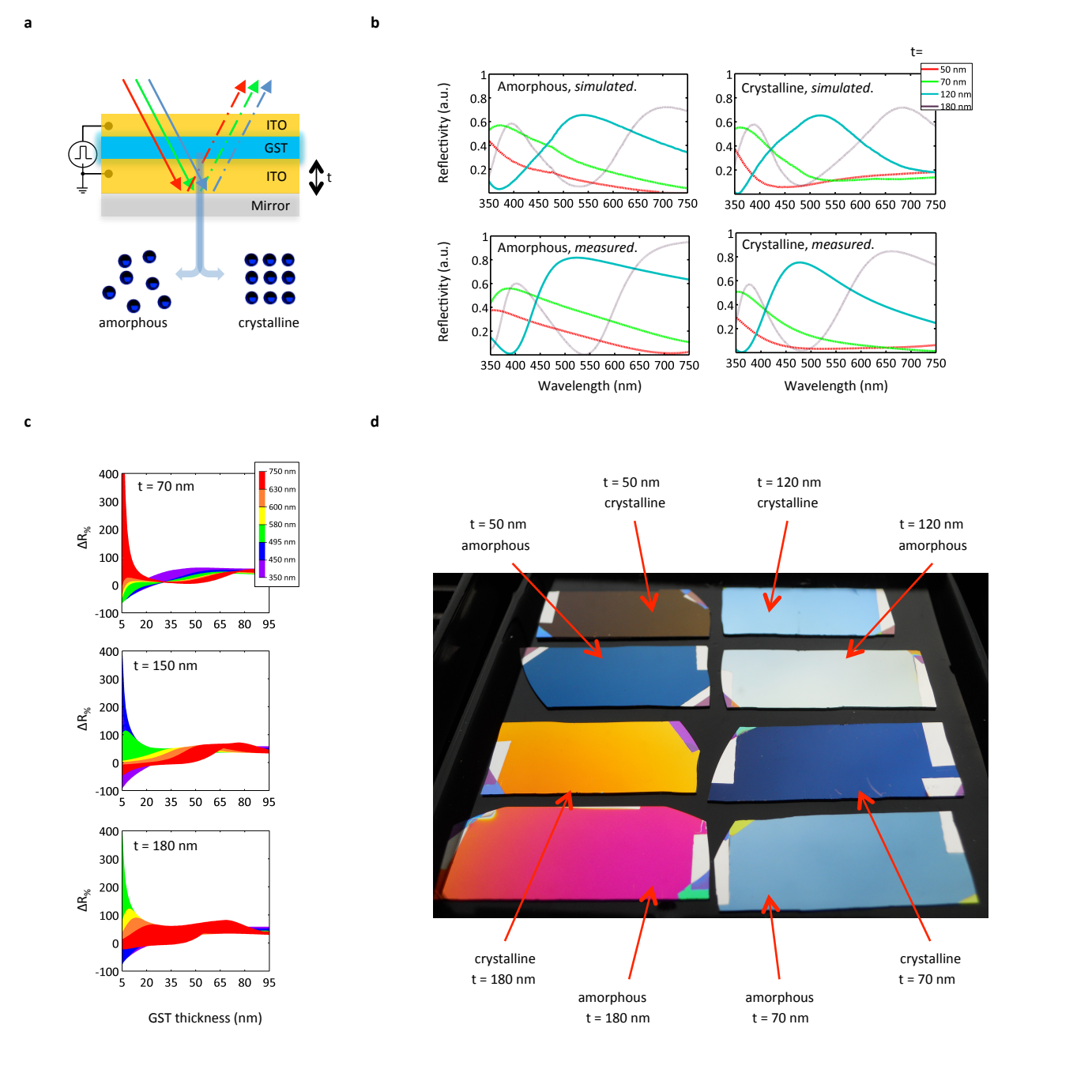
a
ITO
GST
ITO
Mirror
t
amorphous
crystalline
b
t=
50 nm
70 nm
120 nm
180 nm
Amorphous, simulated.
Crystalline, simulated.
Amorphous, measured.
Crystalline, measured.
Reflectivity (a.u.)
Wavelength (nm)
c
t = 70 nm
t = 150 nm
t = 180 nm
750 nm
630 nm
600 nm
580 nm
495 nm
450 nm
350 nm
ΔR%
GST thickness (nm)
d
t = 50 nm
amorphous
t = 50 nm
crystalline
t = 120 nm
crystalline
t = 120 nm
amorphous
crystalline
t = 180 nm
amorphous
t = 180 nm
amorphous
t = 70 nm
crystalline
t = 70 nm

a

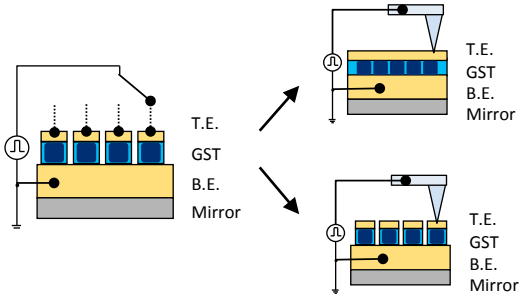
T.E.
GST
B.E.
Mirror
T.E.
GST
B.E.
Mirror
T.E.
GST
B.E.
Mirror

b

c

d

e

f


UNIVERSITY OF
OXFORD

g


UNIVERSITY OF
OXFORD

h

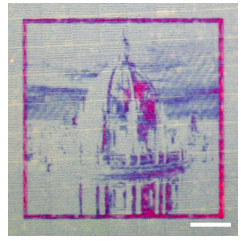

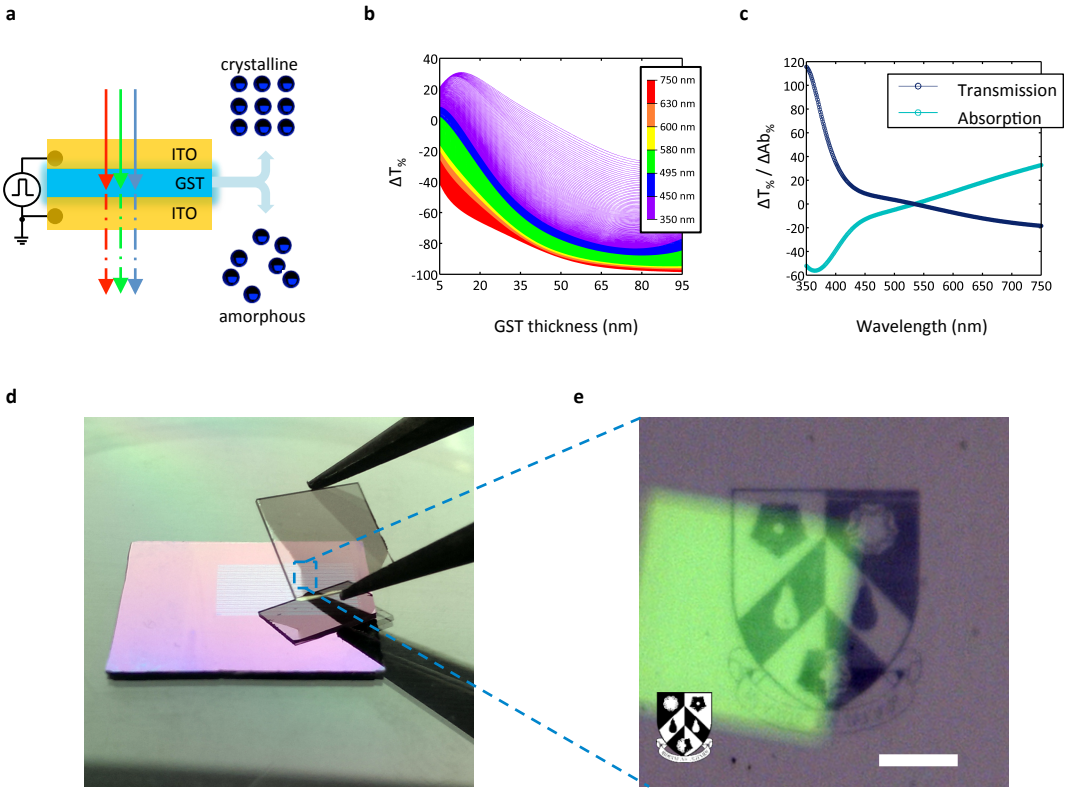
a
crystalline
ITO
GST
ITO
amorphous
b
ΔT%
750 nm
630 nm
600 nm
580 nm
495 nm
450 nm
350 nm
GST thickness (nm)
c
Transmission
Absorption
ΔT% / ΔAb%
Wavelength (nm)
d
e

a

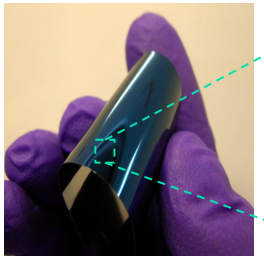

b

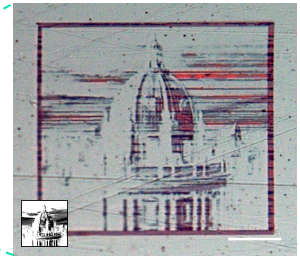

c

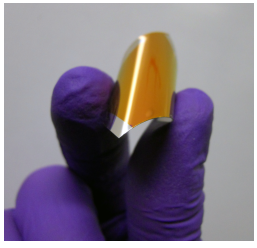

d

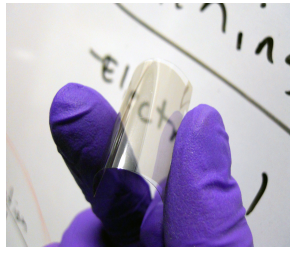

a

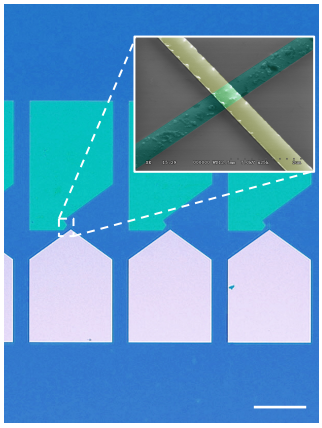

b

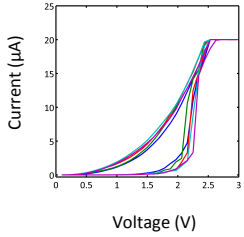

c